# Retraction: Integrative genomics identifies APOE ε4 effectors in Alzheimer's disease

**Article** *in* Nature · July 2013
DOI: 10.1038/nature12415 · Source: PubMed



**6 authors**, including:

Herve Rhinn
Columbia University
**13** PUBLICATIONS **745** CITATIONS
SEE PROFILE

Rong Cheng
Columbia University
**97** PUBLICATIONS **3,385** CITATIONS
SEE PROFILE

Joseph H Lee
Columbia University
**243** PUBLICATIONS **6,819** CITATIONS
SEE PROFILE

ARTICLE

doi:10.1038/nature12415

# Integrative genomics identifies APOE ε4 effectors in Alzheimer's disease

Herve Rhinn[1,2]*, Ryousuke Fujita[1,2]*, Liang Qiang[1,2], Rong Cheng[2], Joseph H. Lee[2,3] & Asa Abeliovich[1,2]

**Late-onset Alzheimer's disease (LOAD) risk is strongly influenced by genetic factors such as the presence of the apolipoprotein E ε4 allele (referred to here as *APOE4*), as well as non-genetic determinants including ageing. To pursue mechanisms by which these affect human brain physiology and modify LOAD risk, we initially analysed whole-transcriptome cerebral cortex gene expression data in unaffected *APOE4* carriers and LOAD patients. APOE4 carrier status was associated with a consistent transcriptomic shift that broadly resembled the LOAD profile. Differential co-expression correlation network analysis of the *APOE4* and LOAD transcriptomic changes identified a set of candidate core regulatory mediators. Several of these—including *APBA2*, *FYN*, *RNF219* and *SV2A*—encode known or novel modulators of LOAD associated amyloid beta A4 precursor protein (APP) endocytosis and metabolism. Furthermore, a genetic variant within *RNF219* was found to affect amyloid deposition in human brain and LOAD age-of-onset. These data implicate an *APOE4* associated molecular pathway that promotes LOAD.**

Alzheimer's disease is the most common form of dementia worldwide, and is characterized by cognitive decline with distinctive brain pathology that includes regional neuron loss, amyloid plaques and neurofibrillary tangles[1]. Rare familial forms of Alzheimer's disease are early in onset and caused by mutations in specific genes[2]. In contrast, the aetiology of common, non-familial LOAD appears much more complex and includes many genetic and environmental factors. The major constituent of amyloid plaques is amyloid beta (Aβ), a proteolytic fragment derived from APP. The observation that familial-associated mutations typically modify Aβ production has led to formulation of the so-called 'amyloid hypothesis', which posits that altered APP processing results in the generation of a toxic fragment that causes neurodegeneration.

Recent genome-wide association studies (GWAS) have implicated common variants at approximately 10 genetic loci in LOAD[3–7]. Individually, these variants have a modest effect on LOAD risk, with the notable exception of the *APOE* ε4 allele (*APOE4*): heterozygosity of *APOE4* is associated with a greater than threefold increase in LOAD risk, when compared to the common *APOE* ε3 allele (referred to here as *APOE3*), and *APOE4* homozygosity increases risk more than tenfold. A third and more rare allele, *APOE* ε2 (referred to here as *APOE2*), appears protective relative to *APOE3* in that carriers of this allele are at reduced risk of LOAD relative to non-carriers. The *APOE4* allele has been shown to modify the tertiary structure of APOE protein, but how this ultimately impacts LOAD is unclear. Various pathogenic mechanisms have been proposed for *APOE4*, including defects in the clearance and degradation of extracellular Aβ, in lipid and cholesterol trafficking, in APP metabolism, in inflammation and in other aspects of neuronal function and survival[8–13].

To pursue molecular pathways that underlie LOAD in an unbiased fashion, whole-transcriptome differential gene expression analyses have been used[14–17]. However, gene expression changes in diseased brain tissue often reflect processes that are secondary to the disease pathology, such as cell loss, rather than causative events. Network approaches, including differential co-expression analysis (DCA)[18–21], have been developed to disentangle causative events from secondary changes within transcriptome-wide gene expression data sets[18,21]. DCA is based on the notion that transcripts encoding causal 'nodes' or 'master regulators' of a disease process—whose activities are critically altered in a pathological state such as LOAD—can be identified by their co-expression correlation network properties, but not by simple differential gene expression analysis. We have broadened existing DCA tools to include consideration of genes other than those encoding known transcription factors[21], with the rationale that DCA nodes would likely include upstream regulators of such factors. DCA ranks most highly those transcripts that are most altered in their co-expression correlation with the greatest number of differentially expressed transcripts in the context of a pathological state such as LOAD (Supplementary Fig. 1).

Here we apply DCA to uncover regulatory mechanisms that affect LOAD and LOAD risk. We first show by differential gene expression analysis that a transcriptome-wide pattern of change is associated with the presence of *APOE4* in disease-free brain tissue, and that this pattern overlaps with the transcriptomic changes that distinguish LOAD affected from unaffected brain tissue. Subsequent DCA identified candidate regulatory node genes predicted to mediate the common transcriptomic changes observed in *APOE4* carriers and LOAD patients. These genes include several known or novel modifiers of APP processing and endocytic trafficking such as *APBA2*, *ITM2B*, *FYN*, *RNF219* and *SV2A*, suggesting a shared mechanism of action. Genetic or pharmacological modulation of these candidate regulatory nodes suppressed altered APP processing in cell models, including *APOE4*-positive human induced neurons (hiNs). Furthermore, meta-analysis of LOAD genome-wide association data indicated that common genetic variants within two such candidate regulatory nodes, *FYN* and *RNF219*, are predictive of LOAD age-of-onset in an *APOE4*-dependent manner. Taken together, our findings reveal an *APOE4*-dependent molecular pathway to LOAD and LOAD risk.

## A pre-LOAD state in *APOE4* carriers

To broadly pursue a molecular correlate of the *APOE4* prodromal state in an unbiased manner, we initially re-evaluated publically available

[1]Departments of Pathology, Cell Biology, and Neurology, Columbia University, 650 W. 168th Street, New York, New York 10032, USA. [2]Taub Institute for Alzheimer's Disease and the Aging Brain, Columbia University, 650 W. 168th Street, New York, New York 10032, USA. [3]Sergievsky Center and Department of Epidemiology, Columbia University, 630 W. 168th Street, New York, New York 10032, USA.
*These authors contributed equally to this work.

transcriptome-wide gene expression data from cerebral cortex autopsy brain tissue of 185 individuals unaffected by LOAD, stratified by their *APOE* genotype (Supplementary Fig. 2, Gene expression omnibus (GEO) accession number GSE15222 (ref. 22)). Hierarchical clustering analysis revealed that the overall pattern of gene expression change associated with all *APOE* high-risk genotypes was closely related to the pattern of change associated with LOAD (relative to other neurological diseases; Fig. 1a).

We next sought to characterize in detail the specific gene expression changes affected by *APOE4* carrier status and to contrast these with changes seen in LOAD brain. To avoid potential confounding effects, LOAD associated changes in brain gene expression were quantified independently of *APOE* variability (by limiting the analysis of LOAD impact to individuals homozygous for *APOE3*); conversely, the transcriptomic effects of *APOE4* carrier status were evaluated independently of the LOAD analysis (by limiting the study to LOAD-unaffected individuals and excluding *APOE3* homozygous samples that were used in the LOAD analysis, Supplementary Fig. 3). Gene expression changes were highly correlated in the two comparisons ($R = 0.62, P = 4 \times 10^{-16}$ by Wald statistics): out of 8,449 gene transcripts detected in all samples, 215 were found to be significantly altered in expression by either *APOE4* or LOAD status in the same direction, whereas 37 were significantly altered in opposite directions (Fig. 1b, c, Supplementary Fig. 4a and Supplementary Table 1). We note that similar analysis of the transcriptomic effect of ageing in LOAD-unaffected individuals (age >85, relative to age <75)—the major non-genetic risk factor for LOAD—revealed a high degree of overlap with LOAD-associated transcriptomic changes, but not with the changes associated with *APOE4* carrier status (Fig. 1c and Supplementary Figs 4b, c and 5). These data suggest that separate mechanisms underlie the effectof *APOE* status and ageing on LOAD risk.

Next, we hypothesized that the overlapping pattern of brain gene expression changes associated either with LOAD or with unaffected APOE high-risk status in brain tissue (termed the *APOE4*/LOAD pattern; defined by a set of 215 transcripts) represented a signature of a pre-LOAD prodrome state (Fig. 1b, c and Supplementary Fig. 3b). Consistent with this, the *APOE4*/LOAD pattern was highly correlated with changes seen in transition from unaffected LOAD-free tissue to incipient-LOAD tissue in an independent data set of cortical tissue transcriptome expression profiles ($R = 0.36$, $P = 9 \times 10^{-4}$ by Wald statistics; rather than the transition from incipient to moderate, or from moderate to severe disease, $R = 0.04$ and 0.02, respectively; Supplementary Fig. 4d).

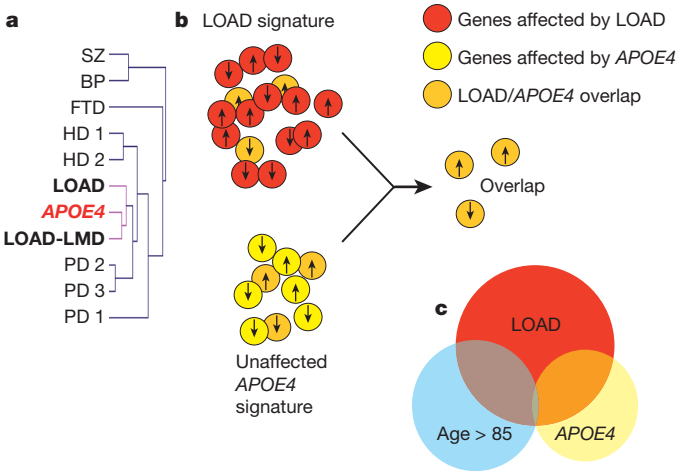


**Figure 1 | Transcriptomic evidence of a pre-LOAD state in unaffected *APOE4* brain tissue.** **a**, Schematic of the overlapping patterns of transcriptome-wide cerebral cortex gene expression changes associated with LOAD or with *APOE4* carrier status. **b**, Hierarchical clustering dendrogram demonstrates similarity between the transcriptome-wide gene expression changes associated with *APOE4* unaffected carrier status and with LOAD. Also presented are the differential expression profiles of LOAD laser-microdissected neurons (LOAD-LMD), bipolar disorder cerebral cortex (BD), schizophrenia cerebral cortex (SZ), fronto-temporal dementia cerebral cortex (FTD), Huntington's disease (in frontal cortex (HD 1) or in caudate nucleus (HD 2)) and Parkinson's disease (in substantia nigra (PD 1), in frontal cortex (PD 2), or in putamen (PD 3)). Analyses used Gene Expression Omnibus (GEO) data sets GSE15222, GSE5281, GSE12649, GSE13162, GSE3790 and GSE20295. **c**, Venn diagram illustrating the overlap in transcriptome-wide gene expression changes in the context of *APOE4*, advanced age (>85 years old) or LOAD.

## *APOE4* and LOAD differential co-expression analysis

Transcriptome-wide differential gene expression analyses, as described above for *APOE4* or LOAD, provide a broad and unbiased molecular perspective of a tissue. However, mechanistic interpretation of individual gene expression changes is challenging, as such changes may represent indirect, downstream consequences of pathology. To address this issue, we applied DCA—a tool for the identification of candidate regulatory node elements that play causal roles in the context of transcriptome-wide gene expression network changes—to the *APOE4*/LOAD pattern of change (Fig. 2a–c and Supplementary Figs 6–9). Among the 20 most highly ranked candidate node elements identified by DCA, we noted that several had previously been implicated in the processing and intracellular sorting of APP, including *APBA2* (ref. 23), *ITM2B* (ref. 24), *TMEM59L* (ref. 25) and *FYN* (ref. 26), suggesting a shared mechanism of action. Consistent with this notion, another top DCA hit, *SV2A*, encodes a well-described regulator of neuronal endocytosis. Furthermore, a selective SV2A inhibitor, the anti-epileptic levetiracetam[27], was recently reported to suppress pathological neuronal hyperactivity in the hippocampus of individuals with mild cognitive impairment (MCI), which precedes LOAD[28]. The top-ranked DCA hit, *RNF219*, had not previously been linked to LOAD, but common genetic variants at the *RNF219* locus had been associated with alternations in lipid metabolism[29], cognitive performance[30] and central nervous system ventricle volume[31], akin to pathological associations ascribed to APOE4.

We sought to test whether DCA candidate node genes (Fig. 2b) may broadly function as regulators of APP processing in an APOE4-dependent manner. To functionally evaluate DCA-identified genes, we initially used a simple *in vitro* model system in which mouse neuroblastoma N2a cells that overexpress a human *APP* transgene (N2a-APP cells) were treated with exogenous APOE protein variants (100 μg ml$^{-1}$ for 18 h). In this APP-N2a model system, treatment with recombinant human APOE ε4 variant protein (rhAPOE4), but not APOE ε2 or APOE ε3 protein (rhAPOE2 or rhAPOE3), significantly increased the levels of extracellular Aβ40 and Aβ42 (Supplementary Fig. 10a). Individual knockdown of several DCA hits by transfection of vectors encoding appropriate small hairpin RNAs (shRNAs; Supplementary Fig. 11a), including *RNF219*, *SV2A*, *HDLBP*, *ROGDI*, *CALU* and *PTK2B*, suppressed the induction of Aβ40 and Aβ42 levels in the context of rhAPOE4 treatment (Fig. 2d and Supplementary Figs 10b–d, 11b–h). With the exception of *HDLBP*, transfection of these knockdown vectors did not affect Aβ levels in the absence of rhAPOE4 (in rhAPOE2- or vehicle-only treated cultures). Thus, the DCA-identified node hits included many known or novel potential modifiers of APOE4-dependent Aβ accumulation.

## *RNF219* and *SV2A* modulate APP processing

We next investigated mechanisms by which DCA-identified genes may mediate the impact of APOE4 on APP processing, and focused on the top two DCA hits: *RNF219* and *SV2A*. Cleavage of APP by the BACE1 β-secretase, a rate-limiting step in Aβ production[32], generates both a soluble extracellular fragment, sAPPβ, and a transmembrane carboxy-terminal fragment (β-CTF), termed C99. rhAPOE4 treatment of N2a-APP cells increased levels of both sAPPβ in cell media and C99 fragment in cell lysates (Fig. 2e, f and Supplementary Fig. 12). Such effects were suppressed by knockdown of either *RNF219* or *SV2A*, pointing to

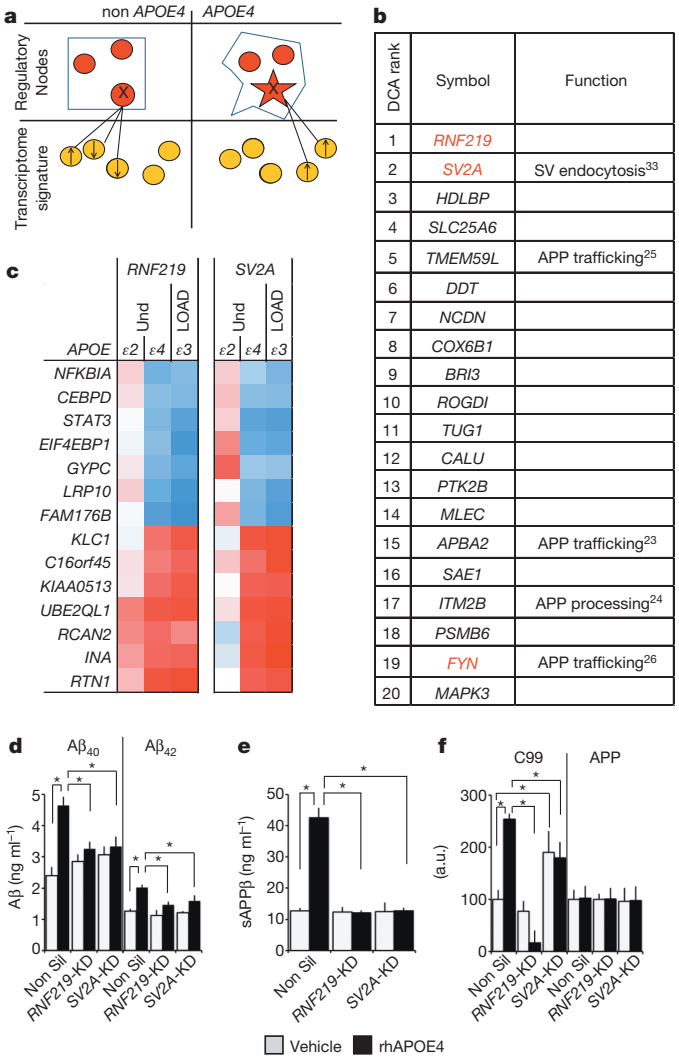


| DCA rank | Symbol | Function |
|---|---|---|
| 1 | *RNF219* | |
| 2 | *SV2A* | SV endocytosis[33] |
| 3 | *HDLBP* | |
| 4 | *SLC25A6* | |
| 5 | *TMEM59L* | APP trafficking[25] |
| 6 | *DDT* | |
| 7 | *NCDN* | |
| 8 | *COX6B1* | |
| 9 | *BRI3* | |
| 10 | *ROGDI* | |
| 11 | *TUG1* | |
| 12 | *CALU* | |
| 13 | *PTK2B* | |
| 14 | *MLEC* | |
| 15 | *APBA2* | APP trafficking[23] |
| 16 | *SAE1* | |
| 17 | *ITM2B* | APP processing[24] |
| 18 | *PSMB6* | |
| 19 | *FYN* | APP trafficking[26] |
| 20 | *MAPK3* | |

**Figure 2 | Differential co-expression correlation analysis of the *APOE4*- and LOAD-associated transcriptomic states.** **a**, Schematic of the DCA model. The pattern of node gene (red) co-expression with differentially expressed genes (yellow) is reconfigured in the context of *APOE4* or LOAD tissue. **b**, Candidate node regulatory genes that underlie the *APOE4*/LOAD pattern of expression changes, rank-ordered by DCA. **c**, Heat maps representing the co-expression correlation coefficients for *RNF219* or *SV2A* with representative genes from the *APOE4*/LOAD pattern set (in rows) as a function of *APOE* genotype and LOAD status (in columns; Und, LOAD-unaffected). High co-expression correlations are denoted in red, high anti-correlations in blue. **d–f**, rhAPOE4 treatment of N2a-APP cells induced the accumulation of APP metabolites including Aβ40, Aβ42 (**d**) and sAPPβ (**e**) in extracellular media, and C99 fragment (**f**) in cell lysates. Such accumulations were suppressed with transfection of shRNA vector-mediated knockdown of *RNF219* or *SV2A* (*RNF219*-KD or *SV2A*-KD, respectively) (relative to non silencing vector control (Non Sil)). Error bars are s.e.m.; $n = 12$, 8 and 8 (**d**, **e**), and 6, 5 and 6 (**f**) independent wells per group for the Non Sil, RNF219-KD and SV2A-KD groups, respectively. $^*P < 0.05$; analyses by ANOVA followed by Student–Newman–Keuls (SNK) test.

increased BACE1 processing as a primary mechanism for the impact of APOE4 on Aβ accumulation, and a regulatory mediator role for SV2A and RNF219 in this context. Neither APP holoprotein nor BACE1 levels were altered in the context of rhAPOE4 treatment or knockdown of these DCA hits.

BACE1 cleavage of APP is most efficient in acidic intracellular compartments such as early and late endosomes[32], and thus one potential mechanism for APOE4 action on APP processing would be through altered APP internalization[11]. We quantified the effect of DCA candidate node knockdown on APP and BACE1 subcellular co-localization in the context of rhAPOE4 stimulation, using either immunocytochemistry (ICC), or by cell-surface protein analysis through selective biotinylation and fractionation. rhAPOE4 treatment of N2a-APP cells shifted both APP and BACE1 localization away from the cell surface and to a common endocytic compartment, leading to increased co-localization (Fig. 3a–d). Such rhAPOE4-induced endocytic co-localization of APP and BACE1 was suppressed by knockdown of the DCA node genes *RNF219* or *SV2A*. Knockdown of *RNF219* appeared to selectively inhibit the internalization of APP in the presence of rhAPOE4, whereas *SV2A* knockdown appeared to have a broader effect on APP internalization, even in the absence of rhAPOE4. Additionally, *SV2A* (but not *RNF219*) knockdown suppressed the internalization of BACE1 in an APOE4-dependent manner (Fig. 3a–d and Supplementary Figs 13, 14).

We further investigated the roles of *SV2A* and *RNF219* in the context of overexpression studies. Transfection of N2a-APP cells with a vector encoding an SV2A enhanced green fluorescent protein fusion protein (SVA2–EGFP)[33] led to increased accumulation of sAPPβ, Aβ40 and Aβ42 species, regardless of the presence of rhAPOE4 (Fig. 3g and Supplementary Fig. 15d, e). Importantly, mutation of a critical tyrosine residue within the endocytosis motif of SV2A, Y46A (ref. 33), that selectively impairs SV2A association with clathrin adaptor proteins but does not affect other activities of SV2A (ref. 33), abrogated the effect of SV2A–EGFP overexpression on APP processing. Furthermore, whereas wild-type SV2A–EGFP co-localized with APP and BACE1, such co-localization was reduced with the Y46A mutant of SV2A–EGFP (Supplementary Fig. 15). These data support a direct role for SV2A-mediated endocytosis in the regulation of APP processing. In contrast with SV2A–EGFP, overexpression of wild-type RNF219–EGFP fusion protein in N2a-APP cells did not appear to significantly alter APP processing. However, overexpression of modified RNF219–EGFP forms that harbour RING-domain missense mutations at highly-conserved cysteines RNF219(C18A/C21A)–EGFP, or a RING-domain deletion RNF219(Δ1–77)–EGFP, suppressed the induction of Aβ40, Aβ42 and sAPPβ levels selectively in the context of rhAPOE4 (Fig. 3g, h and Supplementary Fig. 15). Such RNF219 mutants may act in a dominant-negative fashion to affect APP endocytosis and processing. Taken together, these data further implicate DCA candidate nodes in mediating the effect of APOE4 on APP processing through modified endocytosis.

## Levetiracetam corrects APOE4 phenotypes

We next hypothesized that treatment with levetiracetam, a selective SV2A inhibitor[27] used clinically to treat seizure disorders, could correct APOE4 related alteration in APP processing. Consistent with this, levetiracetam significantly decreased extracellular Aβ42 and Aβ40 levels in rhAPOE4 exposed N2a-APP cells (Supplementary Fig. 16a–c). To extend our analyses to a more physiological context, we next used a set of hiN cultures[34], derived from human skin fibroblasts of *APOE4* carriers or non-carriers. hiN cell cultures from *APOE4* carriers displayed increased APP processing to Aβ42 and Aβ40 and increased APP co-localization with BACE1, relative to non-carriers (Fig. 4), consistent with the N2a studies above. Levetiracetam treatment suppressed the accumulation of Aβ40 or Aβ42 species, as well as APP co-localization with BACE1, selectively in the context of *APOE4* carrier cultures. Thus, SV2A is required for the APOE4 mediated induction of APP processing in the context of human induced neurons that express endogenous levels of these proteins.

## RNF219 genetically interacts with APOE4

The above studies indicated that DCA-identified candidate node genes may function as effectors of APOE4, leading ultimately to LOAD. Thus, a prediction is that common human genetic variants at DCA gene loci may impact the association of APOE4 with LOAD risk or age-of-onset. To this end, single-nucleotide polymorphisms (SNPs) within 50 kilobases of the 20 top-ranking DCA identified genes were each evaluated for their genetic interaction with APOE4 in modulating LOAD age-of-onset, through a meta-analysis of 4 publicly available

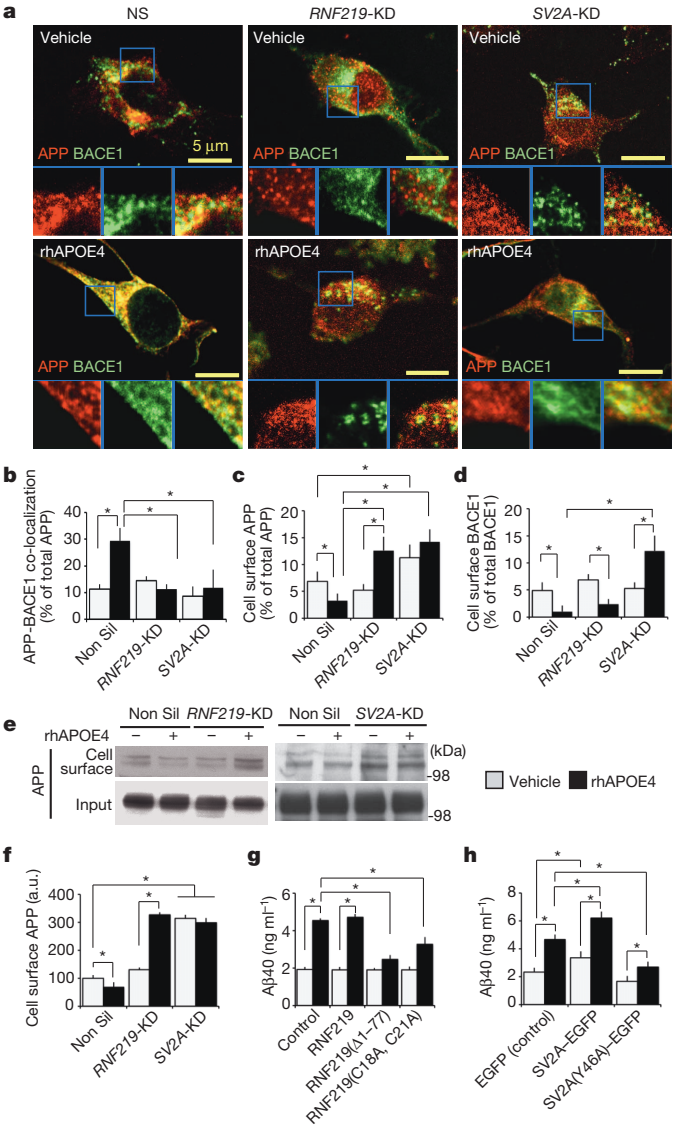


**Figure 3 | RNF219 and SV2A modulate APP proteolytic processing and localization in an APOE4-dependent manner.** **a–d**, ICC analysis of APP and BACE1 co-localization in N2a cells in the context of APOE4 or vehicle, and with transfection of knockdown (KD) vectors for RNF219, SV2A or non silencing vector control (Non Sil); $n = 25$, 24,16,18, 30 and 36 cells in 3 independent wells per group, for the groups Non Sil plus vehicle; Non Sil plus rhAPOE4; *RNF219*-KD plus vehicle; *RNF219*-KD plus rhAPOE4; *SV2A*-KD plus vehicle, and *SV2A*-KD plus rhAPOE4, respectively. Scale bar, 5 μm. **e**, **f**, Biochemical quantification of cell-surface APP upon RNF219 or SV2A knockdown in rhAPOE4-treated N2a-APP cells. a.u, arbitrary units. $n = 6$, 5 and 6 independent wells for the Non Sil, *SV2A*-KD and *rhRNF219*-KD groups, respectively. **g**, **h**, Aβ40 levels in media of N2a-APP cells in the context of RNF219 (**g**) or SV2A–EGFP (**h**) overexpression. $n = 24$, 22, 12, 12, 18 and 18 independent wells for the groups Non Sil plus vehicle, Non Sil plus rhAPOE4, RNF219(wild-type) plus vehicle, RNF219(wild-type) plus rhAPOE4, RNF219(Δ1–77) plus vehicle, and RNF219(Δ1–77) plus rhAPOE4 respectively; $n = 24$, 22, 12, 12, 18 and 18 independent wells for groups Non Sil plus vehicle, Non Sil plus rhAPOE4, SV2A–EGFP plus vehicle, SV2A–EGFP plus rhAPOE4, SV2A(Y46A)–EGFP plus vehicle, and SV2A(Y46A)–EGFP (**g**) respectively. For all figures, error bars are s.e.m., $^*P < 0.05$ by ANOVA followed by Tukey HSD (**a**) or SNK test (**c**, **d**, **f**–**h**).

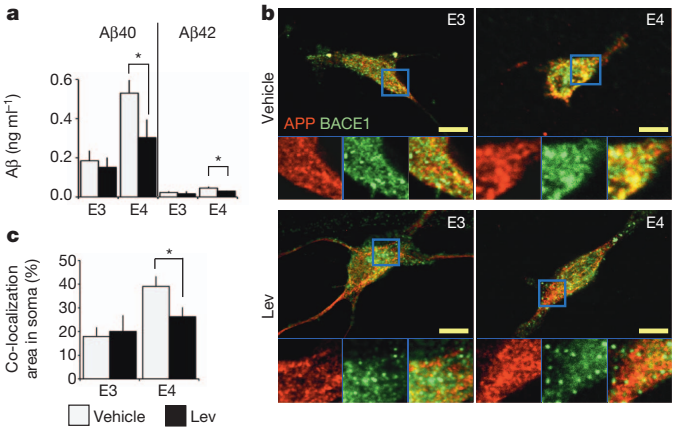


**Figure 4 | SV2A inhibition in human induced neurons modifies APP processing in an APOE4-dependent manner.** **a**, Aβ40 and Aβ42 quantification in media from APOE ε3/ε3 (E3) or APOE ε3/ε4 (E4) hiN cultures treated with levetiracetam (Lev; 1 μM) or vehicle-only. Results represent the means ± s.e.m. ($n = 6$ and 12 independent wells for E3 and E4 groups, respectively). $^*P < 0.05$. Analysis by ANOVA followed by post-hoc Tukey HSD. **b**, **c**, ICC analysis of APP and BACE1 co-localization in APOE3 and APOE4 hiN cultures treated with levetiracetam (1 μM) or vehicle-only. Insets show high-magnification images for visualization of BACE1 and APP co-localization. Means ± s.e.m. are presented (**c**). $n = 40$ (in 4 independent wells), 46 (6 independent wells), 35 (3 independent wells) and 48 (6 independent wells) cells in the groups E3 plus vehicle, E3 plus levetiracetam, E4 plus vehicle and E4 plus levetiracetam, respectively. $^*P < 0.05$ by ANOVA followed by post-hoc analysis with Tukey HSD test. Scale bar, 5 μm.

GWAS data sets: GenADA (875 LOAD cases and 850 controls[35]), TGEN Discovery (446 LOAD cases and 290 controls[36]), TGEN Replication (197 LOAD cases and 114 controls[36]), and ADNI (180 LOAD cases and 214 controls[37]). SNP variants at the *FYN* and *RNF219* loci were associated with significantly decreased LOAD age-of-onset in *APOE4* non-carriers, but not in *APOE4* carriers (Bonferroni corrected $P$ values $= 2.93 \times 10^{-4}$ and $6.03 \times 10^{-3}$, respectively; Fig. 5a, b, Supplementary Fig. 17a and Supplementary Tables 2–4), consistent with a genetic interaction between these DCA hits and APOE4. More broadly, the set of genetic loci that encode DCA 'hits' was found to be enriched for genetic variants modulating LOAD age-of-onset in an APOE4-dependent fashion, as quantified using a gene-set enrichment algorithm (Supplementary Fig. 18 and ref. 38). We note that this was not the case for genes that were identified by simple differential gene expression analysis only, supporting the notion that DCA more efficiently identifies genes with a causal role.

Given the role of *RNF219* in APP processing *in vitro*, we next hypothesized that genetic variants at *RNF219* that are associated with LOAD, such as rs2248663, may also affect central nervous system Aβ accumulation *in vivo* even in unaffected carriers. To this end, we analysed Florbetapir ($^{18}$F) positron emission tomography (PET) imaging, which quantifies central nervous system Aβ amyloid load[39], in a data set of 206 genotyped unaffected elderly individuals (cognitively intact; within the Alzheimer's Disease Neuroimaging Initiative; ADNI[37,40]). As previously described[40], *APOE4* carrier status was strongly associated with increased Aβ amyloid load across multiple brain regions including cingulate, frontal, parietal and temporal cortex. Strikingly, the *RNF219* rs2248663 minor allele was similarly associated with increased Aβ amyloid load within many brain regions including cingulate, frontal, parietal and temporal cortex and brainstem, but not cerebellum ($n = 177$; Supplementary Table 5). When stratified by *APOE* genotype, the *RNF219* genotype significantly affected Aβ load in unaffected *APOE4* non-carriers (*ε3/ε3*; $n = 129$; Fig. 5d). Such an association was not apparent in *APOE4* carriers (*ε3/ε4*; $n = 44$), but could not be entirely excluded due to the more limited power of analysis in the *APOE4* carrier subset. In contrast to such positive findings in unaffected cognitively intact individuals, Aβ amyloid load was not significantly associated with *RNF219* genotype in affected individuals diagnosed with mild cognitive impairment (MCI; $n = 382$ total from the ADNI cohort[40], Supplementary Table 5), regardless of *APOE* genotype. This is consistent with a selective role for *RNF219* that precedes the onset of

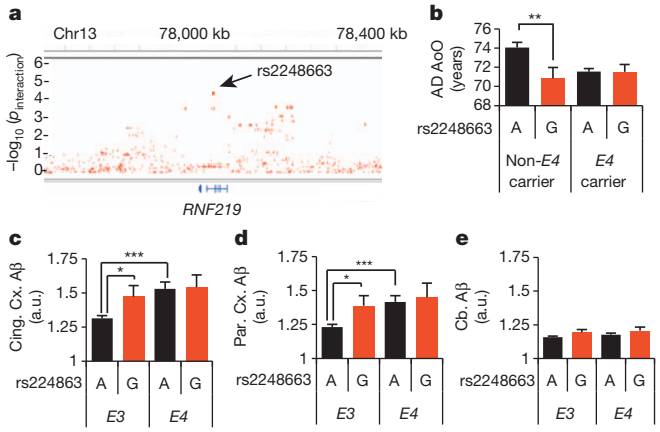


**Figure 5 | An *RNF219* polymorphism modifies LOAD age-of-onset and amyloid deposition in human brain.** **a**, Manhattan plot of the *RNF219* locus presenting the *P* value (log-scale, on *x*-axis) of the interaction between *APOE4* and individual SNPs proximal to the the *RNF219* gene (in blue, vertical bars represent exons) in the LOAD age-of-onset meta-analysis. **b**, Mean LOAD age-of-onset across the TGEN, GenADA and ADNI data sets. Error bars represent s.e.m.; $n = 339$, 67, 530 and 102 individuals for the groups: non APOE4 carrier with RNF219 rs2248663(A); non APOE4 carrier with RNF219 rs2248663(G); APOE4 carrier with RNF219 rs2248663(A); and APOE4 carrier with RNF219 rs2248663(G). $^{**}P < 0.01$ by ANOVA followed by Tukey HSD. **c–e**, Mean Aβ amyloid load in cognitively intact elderly individuals from the ADNI cohort, as quantified by florbetapir-PET within cingulate cortex (**c**), parietal cortex (**d**) or cerebellum (**e**). $n = 129$, 44, 41 and 7 individuals for the groups *APOE3* carrier with *RNF219* rs2248663(A); *APOE3* carrier with *RNF219* rs2248663(G); *APOE4* carrier with *RNF219* rs2248663(A); and *APOE4* carrier with *RNF219* rs2248663(G), respectively. Error bars represent s.e.m.;$^{*}P < 0.05$, $^{***}P < 0.001$ by ANOVA followed by Tukey HSD.

LOAD pathology. Taken together, these findings support a genetic interaction between RNF219 and APOE in the context of Aβ amyloid load in LOAD-unaffected human brain, as well as with respect to LOAD age-of-onset.

## Discussion

Using whole-transcriptome analysis of brain gene expression as a starting point, we describe molecular correlates of a prodromal pre-LOAD state present even in the context of unaffected *APOE4* carriers. Such a prodromal molecular signature is consistent with reports that, even in LOAD-unaffected individuals, APOE4 is nonetheless associated with increased fibrillar Aβ accumulation in the brain[41], decreased cerebrospinal fluid Aβ42 levels[42], and accelerated cognitive decline[43]. As most *APOE4* carriers do not go on to develop LOAD, it is likely that additional unknown 'second hits' are at play.

The candidate mediators identified by DCA herein show limited overlap with prior LOAD transcriptome network analyses, perhaps reflecting differences in experimental design[15,44–47]. For instance, most prior studies have used co-expression approaches primarily to identify clusters of functionally related genes, and subsequently compared the aggregated expression levels of such functional clusters in patient versus unaffected tissue. In contrast, DCA herein was used to identify individual candidate node genes that are highly altered in their patterns of co-expression with all other transcripts in affected tissue. Furthermore, we specifically pursued mechanisms that underlie the early causal events in LOAD, that would be apparent even in unaffected *APOE4* carriers at high risk for LOAD; in contrast, prior network models have often pursued co-expression changes that correspond to disease progression[47].

Levetiracetam was recently shown to improve cognition and reduce hippocampal hyperactivity in individuals with amnestic mild cognitive impairment (aMCI)[28]. Such increased hippocampal activation has also been described in asymptomatic individuals who carry the *APOE4* allele[48]. Levetiracetam treatment of APP transgenic mice has similarly been reported to improve cognitive function, whereas other antiepileptic agents fail to do so[49]. We note that in the absence of transgenic human APOE4, levetiracetam treatment did not modify APP processing in mice[49], consistent with the *in vitro* findings herein. Although the therapeutic action of levetiracetam in patients with aMCI was ascribed to a general suppression of neuronal hyperactivity[28], our data point to a more selective molecular mechanism of action for levetiracetam at SV2A. More broadly, it will be of interest to apply the integrative genomics approaches, as described here, to additional neurological and psychiatric brain disorders.

## METHODS SUMMARY

Differential expression and co-expression analysis were done using the R Bioconductor package essentially as described previously[21]. For knockdown experiments, N2a cells stably expressing human wild-type APP (N2a-APP) were transfected in Opti-MEM1 (Invitrogen) media containing 3 μl of Lipofectamine 2000 (Invitrogen) and an appropriate shRNA expression plasmid (1 μg). Cells were subsequently maintained in DMEM supplemented with 10% FBS, 500 μg ml$^{-1}$ puromycin (A.G. Scientific) and 500 μg ml$^{-1}$ geneticin (Invitrogen) for at least 1 week before phenotypic studies. Aβ quantification by enzyme-linked immunosorbent assay (ELISA) and APP-BACE1 ICC were performed as previously described[34]. Levels of APP holoprotein and BACE1 enzyme at the cell surface were quantified by cell surface biotinylation, fractionation and isolation with Avidin beads, using a Cell Surface Protein Isolation Kit (Pierce) followed by western blot. Human skin fibroblast cultures were obtained from de-identified, banked tissue samples (STC0022: Columbia University Institutional Review Board, IRB #AAAD3566; Primary Investigator Lawrence S. Honig; T-4560: Columbia University Taub Institute New York Brain Bank)[34]. Neurons were induced from the fibroblast cultures by transduction with replication-incompetent lentiviral particles encoding the neurogenic factors *Ascl1*, *Brn2*, *Zic1* and *Myt1l*, in fibroblast media containing polybrene (8 μg ml$^{-1}$)[34]. hiNs were then cultured in glial-conditioned N2 media containing 20 ng ml$^{-1}$ BDNF (Peprotech) and supplemented with dorsomorphin (1 μM; Stemgent) for 4–6 days. Age-of-onset genetic analysis were done by linear regression of age-of-onset as a function of gender, APOE status and the queried genotype, allowing for an interaction term between APOE and the queried SNP minor allele load using gPLINK[50] software. For human Aβ load analysis, Florbetapir (AV-45) PET-scan data was obtained from the ADNI consortium (https://ida.loni.ucla.edu), quantified as standardized uptake value ratio (SUVR)[40]. The effect of rs2248663 or *APOE* genotype on SUVR was evaluated using an additive model within the PLINK linear function, and adjusted for gender and age.

**Full Methods** and any associated references are available in the online version of the paper.

**Received 14 August 2012; accepted 25 June 2013.**
**Published online 24 July 2013.**

1. Selkoe, D. J. Toward a remembrance of things past: deciphering Alzheimer disease. *Harvey Lect.* **99,** 23–45 (2003).
2. Hardy, J. A hundred years of Alzheimer's disease research. *Neuron* **52,** 3–13 (2006).
3. Bertram, L., McQueen, M. B., Mullin, K., Blacker, D. & Tanzi, R. E. Systematic meta-analyses of Alzheimer disease genetic association studies: the AlzGene database. *Nature Genet.* **39,** 17–23 (2007).
4. Harold, D. *et al.* Genome-wide association study identifies variants at CLU and PICALM associated with Alzheimer's disease. *Nature Genet.* **41,** 1088–1093 (2009).
5. Lambert, J. C. *et al.* Genome-wide association study identifies variants at *CLU* and *CR1* associated with Alzheimer's disease. *Nature Genet.* **41,** 1094–1099 (2009).
6. Hollingworth, P. *et al.* Common variants at *ABCA7*, *MS4A6A/MS4A4E*, *EPHA1*, *CD33* and *CD2AP* are associated with Alzheimer's disease. *Nature Genet.* **43,** 429–435 (2011).
7. Naj, A. C. *et al.* Common variants at *MS4A4/MS4A6E*, *CD2AP*, *CD33* and *EPHA1* are associated with late-onset Alzheimer's disease. *Nature Genet.* **43,** 436–441 (2011).
8. Castellano, J. M. *et al.* Human apoE isoforms differentially regulate brain amyloid-beta peptide clearance. *Sci. Transl. Med.* **3,** 89ra57 (2011).
9. Koistinaho, M. *et al.* Apolipoprotein E promotes astrocyte colocalization and degradation of deposited amyloid-β peptides. *Nature Med.* **10,** 719–726 (2004).
10. Mahley, R. W. & Rall, S. C. Jr. Apolipoprotein E: far more than a lipid transport protein. *Annu. Rev. Genomics Hum. Genet.* **1,** 507–537 (2000).
11. He, X., Cooley, K., Chung, C. H., Dashti, N. & Tang, J. Apolipoprotein receptor 2 and X11 α/β mediate apolipoprotein E-induced endocytosis of amyloid-β precursor protein and β-secretase, leading to amyloid-β production. *J. Neurosci.* **27,** 4052–4060 (2007).
12. Ye, S. *et al.* Apolipoprotein (apo) E4 enhances amyloid β peptide production in cultured neuronal cells: apoE structure as a potential therapeutic target. *Proc. Natl Acad. Sci. USA* **102,** 18700–18705 (2005).

13. Huang, Y. Apolipoprotein E and Alzheimer disease. *Neurology* **66,** S79–S85 (2006).
14. Pasinetti, G. M. Use of cDNA microarray in the search for molecular markers involved in the onset of Alzheimer's disease dementia. *J. Neurosci. Res.* **65,** 471–476 (2001).
15. Liang, D. *et al.* Concerted perturbation observed in a hub network in Alzheimer's disease. *PLoS ONE* **7,** e40498 (2012).
16. Gómez Ravetti, M., Rosso, O. A., Berretta, R. & Moscato, P. Uncovering molecular biomarkers that correlate cognitive decline with the changes of hippocampus' gene expression profiles in Alzheimer's disease. *PLoS ONE* **5,** e10153 (2010).
17. Bossers, K. *et al.* Concerted changes in transcripts in the prefrontal cortex precede neuropathology in Alzheimer's disease. *Brain* **133,** 3699–3723 (2010).
18. Hudson, N. J., Reverter, A. & Dalrymple, B. P. A differential wiring analysis of expression data correctly identifies the gene containing the causal mutation. *PLOS Comput. Biol.* **5,** e1000382 (2009).
19. Margolin, A. A. *et al.* ARACNE: an algorithm for the reconstruction of gene regulatory networks in a mammalian cellular context. *BMC Bioinformatics* **7** (suppl. 1), S7 (2006).
20. Presson, A. P. *et al.* Integrated weighted gene co-expression network analysis with an application to chronic fatigue syndrome. *BMC Syst. Biol.* **2,** 95 (2008).
21. Rhinn, H. *et al.* Alternative α-synuclein transcript usage as a convergent mechanism in Parkinson's disease pathology. *Nature Commun.* **3,** 1084 (2012).
22. Webster, J. A. *et al.* Genetic control of human brain transcript expression in Alzheimer disease. *Am. J. Hum. Genet.* **84,** 445–458 (2009).
23. Sano, Y. *et al.* Enhanced amyloidogenic metabolism of the amyloid β-protein precursor in the X11L-deficient mouse brain. *J. Biol. Chem.* **281,** 37853–37860 (2006).
24. Fotinopoulou, A. *et al.* BRI2 interacts with amyloid precursor protein (APP) and regulates amyloid β (Aβ) production. *J. Biol. Chem.* **280,** 30768–30772 (2005).
25. Ullrich, S. *et al.* The novel membrane protein TMEM59 modulates complex glycosylation, cell surface expression, and secretion of the amyloid precursor protein. *J. Biol. Chem.* **285,** 20664–20674 (2010).
26. Hoe, H. S. *et al.* Fyn modulation of Dab1 effects on amyloid precursor protein and ApoE receptor 2 processing. *J. Biol. Chem.* **283,** 6288–6299 (2008).
27. Lynch, B. A. *et al.* The synaptic vesicle protein SV2A is the binding site for the antiepileptic drug levetiracetam. *Proc. Natl Acad. Sci. USA* **101,** 9861–9866 (2004).
28. Bakker, A. *et al.* Reduction of hippocampal hyperactivity improves cognition in amnestic mild cognitive impairment. *Neuron* **74,** 467–474 (2012).
29. Barber, M. J. *et al.* Genome-wide association of lipid-lowering response to statins in combined study populations. *PLoS ONE* **5,** e9763 (2010).
30. Cirulli, E. T. *et al.* Common genetic variation and performance on standardized cognitive tests. *Eur. J. Hum. Genet.* **18,** 815–820 (2010).
31. Furney, S. J. *et al.* Genome-wide association with MRI atrophy measures as a quantitative trait locus for Alzheimer's disease. *Mol. Psychiatry* **16,** 1130–1138 (2011).
32. Vassar, R. *et al.* β-secretase cleavage of Alzheimer's amyloid precursor protein by the transmembrane aspartic protease BACE. *Science* **286,** 735–741 (1999).
33. Yao, J., Nowack, A., Kensel-Hammes, P., Gardner, R. G. & Bajjalieh, S. M. Cotrafficking of SV2 and synaptotagmin at the synapse. *J. Neurosci.* **30,** 5569–5578 (2010).
34. Qiang, L. *et al.* Directed conversion of Alzheimer's disease patient skin fibroblasts into functional neurons. *Cell* **146,** 359–371 (2011).
35. Li, H. *et al.* Candidate single-nucleotide polymorphisms from a genomewide association study of Alzheimer disease. *Arch. Neurol.* **65,** 45–53 (2008).
36. Reiman, E. M. *et al. GAB2* alleles modify Alzheimer's risk in APOE epsilon4 carriers. *Neuron* **54,** 713–720 (2007).
37. Mueller, S. G. *et al.* Ways toward an early diagnosis in Alzheimer's disease: the Alzheimer's Disease Neuroimaging Initiative (ADNI). *Alzheimers Dement.* **1,** 55–66 (2005).
38. Voineagu, I. *et al.* Transcriptomic analysis of autistic brain reveals convergent molecular pathology. *Nature* **474,** 380–384 (2011).
39. Clark, C. M. *et al.* Use of florbetapir-PET for imaging β-amyloid pathology. *J. Am. Med. Assoc.* **305,** 275–283 (2011).
40. Ramanan, V. K. *et al. APOE* and *BCHE* as modulators of cerebral amyloid deposition: a florbetapir PET genome-wide association study. *Mol. Psychiatry* http://dx.doi.org/10.1038/mp.2013.19 (in the press).
41. Reiman, E. M. *et al.* Fibrillar amyloid-β burden in cognitively normal people at 3 levels of genetic risk for Alzheimer's disease. *Proc. Natl Acad. Sci. USA* **106,** 6820–6825 (2009).
42. Morris, J. C. *et al. APOE* predicts amyloid-beta but not tau Alzheimer pathology in cognitively normal aging. *Ann. Neurol.* **67,** 122–131 (2010).
43. Dik, M. G. *et al.* Memory complaints and APOE-ε4 accelerate cognitive decline in cognitively normal elderly. *Neurology* **57,** 2217–2222 (2001).
44. Miller, J. A., Oldham, M. C. & Geschwind, D. H. A systems level analysis of transcriptional changes in Alzheimer's disease and normal aging. *J. Neurosci.* **28,** 1410–1420 (2008).
45. Ray, M. and Zhang, W. Analysis of Alzheimer's disease severity across brain regions by topological analysis of gene co-expression networks. *BMC Syst. Biol.* **4,** 136 (2010).
46. Soler-López, M., Zanzoni, A., Lluís, R., Stelzl, U. & Aloy, P. Interactome mapping suggests new mechanistic details underlying Alzheimer's disease. *Genome Res.* **21,** 364–376 (2011).
47. Zhang, B. *et al.* Integrated systems approach identifies genetic nodes and networks in late-onset Alzheimer's disease. *Cell* **153,** 707–720 (2013).
48. Bookheimer, S. Y. *et al.* Patterns of brain activation in people at risk for Alzheimer's disease. *N. Engl. J. Med.* **343,** 450–456 (2000).
49. Sanchez, P. E. *et al.* Levetiracetam suppresses neuronal network dysfunction and reverses synaptic and cognitive deficits in an Alzheimer's disease model. *Proc. Natl Acad. Sci. USA* **109,** E2895–E2903 (2012).
50. Purcell, S. *et al.* PLINK: a tool set for whole-genome association and population-based linkage analyses. *Am. J. Hum. Genet.* **81,** 559–575 (2007).


**Supplementary Information** is available in the online version of the paper.

**Acknowledgements** We thank R. Mayeux, G. Di Paulo, S. Small and A. Rosenthal for comments on the manuscript; D. Holtzman and J. Cirrito for antibody reagents; and S. Bajjalieh and J. Yao for SV2A expression vectors. We are especially grateful to the many laboratories who contributed data sets included in this study. The work was supported by grants from the National Institutes of Health (NIH) (R01AG042317 and RO1NS064433). J.H.L. and R.C. were partially funded by R37 AG015473 and R01 MH084995. Additionally, data collection and sharing for this project was funded by the Alzheimer's Disease Neuroimaging Initiative (ADNI) (NIH grant U01 AG024904). ADNI is funded by the National Institute on Aging, the National Institute of Biomedical Imaging and Bioengineering, and through generous contributions from the following: Alzheimer's Association; Alzheimer's Drug Discovery Foundation; BioClinica; Biogen Idec; Bristol-Myers Squibb; Eisai; Elan Pharmaceuticals; Eli Lilly; F. Hoffmann-La Roche and its affiliated company Genentech; GE Healthcare; Innogenetics, NV; IXICO; Janssen Alzheimer Immunotherapy Research and Development; Johnson and Johnson Pharmaceutical Research and Development; Medpace; Merck; Meso Scale Diagnostics; NeuroRx Research; Novartis; Pfizer; Piramal Imaging; Servier; Synarc; and Takeda Pharmaceutical Company. The Canadian Institutes of Health Research is providing funds to support ADNI clinical sites in Canada. Private sector contributions are facilitated by the Foundation for the National Institutes of Health (http://fnih.org). The grantee organization is the Northern California Institute for Research and Education, and the study is coordinated by the Alzheimer's Disease Cooperative Study at the University of California, San Diego. ADNI data are disseminated by the Laboratory for Neuro Imaging at the University of California, Los Angeles. This research was also supported by NIH grants P30 AG010129 and K01 AG030514.

**Author Contributions** A.A., H.R. and R.F. designed studies, interpreted data and wrote the manuscript. H.R. performed the bioinformatics and genetic analysis. R.F. performed the cell culture and biochemistry experiments. L.Q. participated in the generation of hiNs. R.C. and J.H.L. provided support for the genetic analysis. Data used in preparation of this article were obtained from the Alzheimer's Disease Neuroimaging Initiative (ADNI) database (http://adni.loni.ucla.edu). As such, the investigators within the ADNI contributed to the design and implementation of ADNI and/or provided data but did not participate in analysis or writing of this report. A complete listing of ADNI investigators can be found at (http://adni.loni.ucla.edu/wp-content/uploads/how_to_apply/ADNI_Acknowledgement_List.pdf).

**Author Information** Reprints and permissions information is available at www.nature.com/reprints. The authors declare no competing financial interests. Readers are welcome to comment on the online version of the paper. Correspondence and requests for materials should be addressed to A.A. (aa900@columbia.edu).

## METHODS

**Materials.** Levetiracetam was obtained from LKT Laboratories, puromycin was purchased from AG Scientific. Recombinant human APOE2 (rhAPOE2), APOE3 (rhAPOE3), and APOE4 (rhAPOE4) were from BioVision. Antibodies obtained were anti-APP C terminus and anti-RNF219 (both rabbit polyclonals, Sigma-Aldrich), anti-APP N-terminal (mouse monoclonal, 22C11, Millipore), anti-APP C-terminal (mouse monoclonal, 2.F2.19B4; from Millipore, for detection of the exogenous human wild-type APP transgene and cleavage products), Anti-APP C-terminal (mouse monoclonal, c1/6.1; Covance, for detection of the endogenous murine APP and cleavage products), anti-beta amyloid (mouse monoclonals, 4G8, 6E10; Covance), anti-BACE1 (rabbit polyclonal; Invitrogen) and anti-RNF219 (rabbit polyclonal; Santa Cruz Biotechnology).

**Cell culture and shRNA expression vector transfection.** N2a cells stably expressing human APP wild type (N2a-APP) were maintained in DMEM supplemented with 10% FBS and 1% penicillin 1% streptomycin and 500–1,000 μg ml$^{-1}$ geneticin (Invitrogen). For knockdown experiments, cells grown overnight to 70–90% confluency in 24-well plates were transfected in Opti-MEM1 (Invitrogen) media containing 3 μl of Lipofectamine 2000 (Invitrogen) and 1 μg of shRNA expressing plasmid DNA and incubated in DMEM supplemented with 10% FBS and 500 μg ml$^{-1}$ puromycin (A.G. Scientific) and 500 μg ml$^{-1}$ geneticin (Invitrogen) at least for 1 week before further experiments. Validated shRNA plasmids were obtained from Open biosytems (pGIPZ backbone): *SV2A* (#1:V3LMM_450995, 5′-TATTGTGC AGGAACGTGCT-3′; #2: V3LMM_450996, 5′-TGATGAACGTGCAGTTGCG-3′; #3:V3LMM_451000, 5′-TGCGGAAGAATGTGTTGCT-3′), *RNF219* (V3LMM_ 483077, 5′-ATCACTTCGTTCTAGAGCT-3′) or Sigma (pLKO backbone): *NCDN* (TRCN0000119418, 5′-CGTAGGATCTTTGATGCCGTT-3′), *CALU* (TRCN00 00114827, 5′-GCTCAGCGATAAAGTTCACAA-3′), *FYN* (TRCN0000023379, 5′-GCTCGGTTGATTGAAGACAAT-3′), *TMEM95L* (TRCN0000178059, 5′-GCTTATTGACATTCCTCACAT-3′), *MAPK3* (TRCN0000023186, 5′-CCATGA GAATGTTATAGGCAT-3′), *HDLBP* (TRCN0000105171, 5′-GCTCGCATTAA GAAGATTTAT-3′), *RNF219* (TRCN0000125455, 5′-CCACGAGATGAGTGA AGATTT-3′), *ROGDI* (TRCN0000012233, 5′-CCCTCCTCATTCCCTGTGGTA-3′).

**Aβ ELISA.** Aβ quantification was performed by ELISA as described previously[34,51]. Media was conditioned for 48 h before harvesting. Samples were analysed for Aβ40 or Aβ42 using specific sandwich ELISAs. Briefly, Aβ40, and Aβ42 were captured using monoclonal antibodies targeted against amino acids 35–40 (HJ2.0), or 33–42 (HJ7.4) of Aβ, respectively. The antibodies HJ2.0, HJ5.1 and HJ7.4 were gifts from D. M. Holtzman. For Aβ40 and Aβ42 assays, a biotinylated central domain monoclonal antibody (HJ5.1) followed by streptavidin-poly-HRP-40 was used for detection (Sigma). All assays were developed using Super Slow ELISA TMB (Sigma) and read on a VersaMax ELISA Microplate Reader (Molecular Devices) at 650 nm. ELISA signals were reported as the mean ± s.e.m. of three replica wells in ng of Aβ per ml of supernatant, based on standard curves using synthetic human and mouse recombinant Aβ40 and Aβ42 peptides (rPeptide; Bogart, GA). Samples were optimized to detect Aβ40 and Aβ42 in the range of 1–3,000 and 0.03–30 ng ml$^{-1}$, respectively[34]. The amount of Aβ was normalized to total cell protein levels.

**Quantitative real time RT–PCR.** qRT–PCR was done as described previously[52]. mRNA levels were quantified using ΔΔCt methods, using GAPDH as a normalizing factors. Forward/reverse primers pairs used were 5′-AGGTCGGTGTGAA CGGATTTG-3′/5′-GGGGTCGTTGATGGCAACA-3′ for *GAPDH*, 5′-GTGCCA CATTTGCTTGGGG-3′/5′-TCAGGAGTGATCGGGACTCTG-3′ for *RNF219*, 5′-AGGTGAAAGGGACTCTGACTC-3′/5′-GCCAAGTGCAACAACTGGT-3′ for *ROGDI*, 5′-AATGCTGATGGGTTCATTGATCT-3′/5′-GGTTCTTATCTC GAAACTCCACG-3′ for *CALU*, 5′-ACAGTGCAGACAGAGATCCAG-3′/5′-CGGATTTGAAGGTCATACCTCCA-3′ for *PTK2B*, 5′-CTCAGGTGTTTCAT GTACCCC-3′/5′-TCAAGGCAGATTTTTGCTTGTTC-3′ for *HDLBP*, 5′-GGT TCACCTTTCCCAACCGA-3′/5′-GCTGGCTAGTTCAGGGTCG-3′ for *NCDN* and 5′-TCCGCCATGAGAATGTTATAGGC-3′/5′-GGTGGTGTTGATAAGC AGATTGG-3′ for *MAPK3*.

**Immunohistochemistry.** Immunocytochemistry (ICC) was performed as previously described[34]. Cells were fixed with 4% paraformaldehyde for 10 min at room temperature, followed by rinsing 3 times with phosphate-buffered saline (PBS). Cells were then permeabilized with 0.3% Triton X-100 in 1× PBS for 2 min at room temperature. After rinsing three times with PBS, cells were incubated with blocking buffer containing 1% BSA and 1% normal goat serum at room temperature for 1 h. All primary antibodies were diluted in blocking buffer. Cells were incubated with primary antibodies (1:200 to 1,500) at 4 °C for 12–16 h, followed by the corresponding secondary antibody solutions at room temperature for 1 h. Cells were rinsed with 1× PBS three times followed by mounting on coverslips with Fluoro-Gel (Electron Microscopy Sciences). Detailed antibody sources and dilutions used can be found in the Supplementary Information. Imaging was conducted by laser-scanning confocal microscopy with a ×63 (1.4 NA) objective (LSM510, Carl Zeiss). Cell counts and fluorescence intensities were quantified in 10 to 35 images of randomly selected views per well. Subsequently, images were analysed for cell counts and fluorescent intensity using Image J 1.42q software (National Institutes of Health).

**Immunoblotting.** Cells were suspended in RIPA buffer contained protease inhibitor cocktail (Sigma) and sonicated, then cells were incubated for 1 h at 4 °C. The lysates were cleared by centrifugation at 10,000*g* for 10 min at 4 °C. Protein concentration was determined by Bio-Rad Dc Protein assay kits (Bio-Rad), 5–30 μg of total protein lysate was resolved on a 4–12% SDS–PAGE gel. Protein samples were transferred onto nitrocellulose membranes using the semi-dry transfer unit (Owl Scientific) and blocked with 3% skimmed milk in Tris buffered saline with 0.1% Tween 20 for 1 h. The primary antibodies were incubated overnight at 4 °C, and primary antibody binding was detected using horseradish peroxidase conjugated anti-mouse IgG at 1:5,000 dilution (Jackson Immunoresearch Laboratories) or horseradish peroxides conjugated anti-rabbit IgG at 1:5,000 dilution (Jackson Immunoresearch Laboratories).

**Cell surface biotinylation.** Levels of APP holoprotein and BACE1 at the cell surface were quantified using cell surface biotinylation followed by fractionation and western blotting. Cell surface biotinylation was performed using a cell surface protein isolation kit following the manufacturer's instructions (Pierce). N2a cell cultures in two 10-cm dishes at 90–95% confluence were first rinsed three times with ice-cold culture medium and then incubated in PBS containing 1 mg ml$^{-1}$ of EZ-link Sulfo NHS-LC biotin (Pierce Chemical), or PBS alone, for 30 min at 4 °C. To quench any excess biotin, cell cultures were rinsed and then incubated in quenching solution for 10 min at 4 °C. Next, cells were gently scraped into conical tubes and centrifuged. Pellets were washed in cold PBS three times, and lysis buffer with protease inhibitor at 4 °C added as per manufacturer's instructions. Cells were sonicated for disruption and incubated 30 min on ice. After incubation, sample were centrifuged 10,000*g* for 2 min and supernatants were collected. Cell lysates from biotin-labelled and unlabelled samples were incubated with NeutrAvidin-agarose beads (Pierce Chemical) for 60 min at room temperature. Subsequently, beads were washed with RIPA buffer containing protease inhibitor cocktail (Sigma), and total protein levels were determined using a BCA protein quantification assay kit (Bio-Rad). For western blot analysis, lysates were mixed with sample buffer, boiled for 10 min, and then resolved on an SDS–PAGE gel. Total protein, containing 15 μg of lysate was simultaneously resolved on the gel, transferred to PVDF membrane and probed for APP and BACE1 expression.

**Human skin fibroblasts.** Human skin fibroblast cultures used in this study were obtained from de-identified, banked tissue samples; there was no interaction with subjects, no intervention, and private, identifiable information was not collected. One fibroblast line was obtained from an unaffected individual homozygous for the *APOE3* allele (STC0022 (female, 65 years old)), and a second line from an unaffected individual who carries one *APOE4* and one *APOE3* allele (T-4560 (male, 89+ years old)). STC0022 and T-4560 were obtained from de-identified, banked tissue samples (STC0022: Columbia University Institutional Review Board, IRB #AAAD3566; Primary Investigator. Lawrence S. Honig; T-4560: Columbia University Taub Institute New York Brain Bank)[34]. Human skin fibroblasts were cultured in standard fibroblast media (DMEM with 10% FBS).

**hiN cell induction and transfection.** Fibroblasts were plated at 20,000 cells per well in 24-well plates one day before infection. Culture plates and dishes were treated with poly-L-ornithine (Sigma) and laminin (Invitrogen) or poly-D lysine (Trevigen) and laminin before the application of the cells as per the manufacturer's instructions. Fibroblasts were transduced with replication-incompetent, VSVg-coated lentiviral particles encoding Ascl1, Brn2, Zic 1 and Myt1l, in fibroblast media containing polybrene (8 μg ml$^{-1}$). Each lentiviral type was added at a multiplicity of infection ~2:1. Two day after transduction, the media was replaced with glial-conditioned N2 media containing 2 ng ml$^{-1}$ BDNF (Peprotech). For the first 4–6 days in N2 media, dorsomorphin (1 μM; Stemgent) was applied to the culture. Media was changed every 2–3 days for the duration of the culture period.

**Differential expression.** The microarray data set was downloaded from the Myers laboratory website. All subsequent data manipulations and analyses were done using R Bioconductor package. For each gene, differential expression between two conditions was assessed by a two-tailed *t*-test, using a threshold *P*-value of 0.05. For a gene to be considered affected by both *APOE* genotype and AD phenotype, its expression level has to be significantly changed in the same direction when comparing samples from unaffected *APOE4* individuals to unaffected *APOE2* individuals and when comparing samples from AD *APOE3* patients to unaffected *APOE3* individuals. Genes annotation enrichment were queried using GSEA[53] or the DAVID bioinformatics resources[54,55].

**Differential wiring analysis.** The microarray data set was downloaded from the Myers laboratory website. All subsequent data manipulations and analyses were done using R Bioconductor package. Correlations between gene expression levels were assessed using cosine similarity on log-transformed levels; briefly, two genes whose expression levels are simultaneously high or low across many samples are

in phase and will have a correlation coefficient close to 1. On the contrary, if one gene shows high expression levels when another one shows low across many samples, those two genes are in anti-phase and will have a correlation coefficient close to −1. The absence of linear relationship between the expression levels of both genes will result in a correlation coefficient close to 0. Comparisons between correlations obtained in two independent groups were done using a Fisher's Z transformation followed by a statistical test using pnorm R function.

The principle underlying DW algorithms[18,56] is that for a given candidate 'master regulator' node gene X, the global DW score—when comparing two experimental conditions 1 and 2—is the sum of DW subscores between gene X and each of the other genes Gi queried. The subscore between the gene of interest X (for which the DW score is calculated) and a gene Gi is proportional to: (1) the extent of the shift in correlation between the expression levels of Gi and X when comparing conditions 2 and 1 (thus genes exhibiting a high number of strong shifts in correlation with many other genes are assumed to be relevant nodes in the differential gene expression network between conditions 1 and 2); (2) the extent of differential expression of Gi between conditions 1 and 2 (averaged across the panel of samples for each condition; thus, the more a gene is on average differentially expressed between 2 conditions, the more it is predicted to have a phenotypic impact); (3) the level of expression Gi (a more highly expressed gene is thought to have a higher phenotypic impact; this is to compensate for the fact that lowly expressed genes are more likely to exhibit strong shifts in expression between the two conditions).

The three main modifications we introduce to the previously described wiring algorithms[18,56] are: (1) We broadened the analysis of possible 'master regulator' genes from only annotated transcription factors to all genes. (2) We introduced significance threshold tests for the interactor genes: as we included all the genes as candidate 'master disease regulators', instead of only all the annotated transcription factors we wanted to avoid artificial results when working at a genome-wide scale than with hundreds of selected genes. Low-selective threshold ($P$ value = 0.05) were however chosen to keep a high sensitivity. (3) We considered for differential expression as well as for differential correlation the intersection between 2 comparisons involving 4 independent groups. For a gene to be considered as differentially expressed, it has to be significantly differentially expressed in both conditions with the same orientation.

The differential wiring score for a gene X between for two comparisons each between two independent experimental groups (1 and 2 with $n_1$ and $n_2$ elements and A and B with $n_A$ and $n_B$ elements, respectively) was thus calculated as the sum over all the genes Gi of the absolute value of the product of: (1) The conditional Z-distance evaluating the difference observed between the two groups in each of the two comparisons for the correlation between the expression levels of genes X and Gi $\left\langle \Delta_{Gi(1vs2)\cap(AvsB)} \right\rangle_p$ in the formal DW formula below. Thus, for a given threshold $P$ value (0.05 here), it has a null value if the correlation shift is not significant. The amplitude of the Z-distance is proportional to the shift in correlation between the two experimental conditions. Fisher's Z-transformation corrects for the non-normal distribution of the correlation value (between −1 and 1). As a consequence, a shift in correlation form 0.7 to 0.9 will lead a Z-distance value higher than a shift from −0.1 to 0.1. (2) The conditional log-scaled amplitude of the differential expression of gene Gi $\left\langle \delta(X,G_i)_{(1vs2)\cap(AvsB)} \right\rangle_p$ in the DW formula below. For a given threshold $P$ value (0.05 here), it has a null value if the gene is found to not be differentially expressed between the two conditions. If the gene is differentially expressed for the chosen $P$ value, the value will be the log of the ratio between the averaged gene expression levels in each group. (3) The averaged expression level of gene Gi among all samples $\overline{(E_{G_i})_{1\cup 2\cup A\cup B}}$ in the formula below.

As a consequence of the use of significance threshold tests, only those genes which are differentially expressed between the two experimental conditions, and that see their correlation with gene X significantly changed between the two experimental conditions, will participate in the DW score.

Formally, the DW score was thus calculated as:
Differential wiring score for gene X:

$$DW(X)_{1vs2} = \sum Gi \left| \left\langle \Delta_{Gi(1vs2)\cap(AvsB)} \right\rangle_p \right| \left\langle \delta(X,G_i)_{(1vs2)\cap(AvsB)} \right\rangle_p \overline{|(E_{G_i})_{1\cup 2\cup A\cup B}}$$

With:
Conditional Z-distance for a p-value p:

$$\langle \delta_{1vs2} \rangle_p = \begin{cases} \sqrt{\delta_{1vs2} \cdot \delta_{AvsB}} & \text{IF pnorm}(\delta_{1vs2}) < p \\ & \text{AND pnorm}(\delta_{AvsB}) < p \\ & \text{AND } \delta_{1vs2} \cdot \delta_{AvsB} \\ 0 & \text{OTHERWISE} \end{cases}$$

$$\delta(X,G)_{1vs2} = \frac{F_z(r(X,G)_1 - F_z(r(X,G)_2)}{\sqrt{\frac{1}{n_1 - 3} + \frac{1}{n_2 - 3}}} \text{ Z-distance between } r(X,G)_1 \text{ and } r(X,G)_2$$

$$\delta(X,G)_{AvsB} = \frac{F_z(r(X,G)_A - F_z(r(X,G)_B)}{\sqrt{\frac{1}{n_A - 3} + \frac{1}{n_B - 3}}} \text{ Z-distance between } r(X,G)_1 \text{ and } r(X,G)_2$$

$r(X,G)_1$, $r(X,G)_2$, $r(X,G)_A$, $r(X,G)_B$ correlation coefficient between the expression levels of genes X and G, evaluated in experimental groups 1 ($n_1$ elements), 2 ($n_2$ elements), A ($n_A$ elements) B ($n_B$ elements).

$$F_Z(r) = \frac{1}{2}\log\left(\frac{1+r}{1-r}\right) \text{ Fisher's z transformation for a correlation coefficient r}$$

Conditional differential gene expression amplitude of Gi

$$\left\langle \Delta_{G_i(1vs2)\cap(AvsB)} \right\rangle_p = \begin{cases} \sqrt{\log\left(\frac{\overline{(E_G)_1}}{\overline{(E_G)_2}}\right) \cdot \left(\frac{\overline{(E_G)_A}}{\overline{(E_G)_B}}\right)} & \text{IF p. value } \left(\text{t.test}\left((E_G)_1,(E_G)_2\right)\right) < p \\ & \text{AND p. value } \left(\text{t.test}\left((E_G)_A,(E_G)_B\right)\right) < p \\ & \text{AND } \log\left(\frac{\overline{(E_G)_1}}{\overline{(E_G)_2}}\right) . \log\left(\frac{\overline{(E_G)_A}}{\overline{(E_G)_B}}\right) > 0 \\ 0 & \text{OTHERWISE} \end{cases}$$

$(E_G)_i$: collection of the expression level values for gene G among an experimental group i. All calculations were performed using the R statistical environment.

**GWAS epistasis analysis.** We used 4 publicly available GWAS data sets; GenADA study was downloaded from NCBI's dbGap repository[57] (Multi-Site Collaborative Study for Genotype–Phenotype Associations in Alzheimer's disease and Longitudinal follow-up of Genotype–Phenotype Associations in Alzheimer's disease and Neuroimaging component of Genotype–Phenotype Associations in Alzheimer's disease, dbGap phs000219.v1.p1), which includes 875 AD cases and 850 controls[35]. Two Tgen neuropathological data sets were obtained from the Translational Genomics Research Institute (http://www.tgen.org). The 'discovery cohort' includes 446 AD cases and 290 controls, the 'replication cohort' 197 AD cases and 114 controls[36]. The ADNI data sets were downloaded from the Alzheimer's Disease Neuroimaging Initiative website (https://ida.loni.ucla.edu) and includes 180 AD cases and 214 controls[37]. All subsequent genetic analysis were done using gPLINK[50] software. Interaction between different SNPs and APOE4 in each data set were evaluated using PLINK linear and interaction functions, applied to the following model $AoO = a + b.APOE + c.Sex + d.SNP + e.\ SNPxAPOEbin$, where $AoO$ is the age-of-onset of Alzheimer's disease, $APOE$ is the allelic load of $APOE\ \varepsilon 4$ allele (= 0, 1 or 2), $Sex$ is the gender (= 0 or 1), $SNP$ the allelic load of the minor allele for the studied SNP (= 0, 1 or 2) and $APOEbin$ a binary indicator for the presence or absence of at least one $APOE4$ allele (= 0 or 1). The term e is considered as the interaction term in the current analysis. Rare $APOE2$ allele carriers were not considered in the present study. Analysis was performed independently in each data set, and then combined in a meta-analysis using METAL (http://www.sph.umich.edu/csg/abecasis/metal/).

**AD age-of-onset GWAS set enrichment analysis.** GWAS enrichment analysis was performed essentially as previously described[38], using the $P$ value resulting from the $APOE4$-dependent AD age-of-onset association meta-analysis described above. For each gene present in the gene expression data set the associated $P$ value corresponds to the lowest meta-analysis $P$ value for a SNP located within 50-kb on either side of the gene, using the 286,178 SNPs present in at least 3 of the 4 studies used in the meta-analysis. A gene set enrichment score was calculated for the different groups of genes considered using a weighted Kolmogorov–Smirnov–like running-sum statistic as previously described[38]. For each gene set, a null distribution was generated by permuting 10,000 times the gene labels, and was used to evaluate an empirical $P$ value for the enrichment score. All calculations were made using R statistical software.

**Florbetapir (AV-45) PET-scan epistasis analysis.** Data was downloaded from the Alzheimer's Disease Neuroimaging Initiative website (https://ida.loni.ucla.edu) and includes data from 177 cognitively intact and 338 mildly cognitively impaired elderly genotyped individuals. Briefly, Aβ load was evaluated by florbetapir-PET and quantified as a standardized uptake value ratio (SUVR)[40] in different brain regions (parietal cortex, cingulate cortex, frontal cortex, temporal cortex, brainstem and cerebellum). The effect of rs2248663 minor allele (G) or $APOE4$ allele

load on the SUVR was evaluated for each group using an additive model within the PLINK linear function, and adjusted for gender and age.


51. Cirrito, J. R. *et al. In vivo* assessment of brain interstitial fluid with microdialysis reveals plaque-associated changes in amyloid-β metabolism and half-life. *J. Neurosci.* **23,** 8844–8853 (2003).
52. Rhinn, H. *et al.* Housekeeping while brain's storming Validation of normalizing factors for gene expression studies in a murine model of traumatic brain injury. *BMC Mol. Biol.* **9,** 62 (2008).
53. Subramanian, A. *et al.* Gene set enrichment analysis: a knowledge-based approach for interpreting genome-wide expression profiles. *Proc. Natl Acad. Sci. USA* **102,** 15545–15550 (2005).
54. Huang D. W., Sherman, B. T. & Lempicki, R. A. Bioinformatics enrichment tools: paths toward the comprehensive functional analysis of large gene lists. *Nucleic Acids Res.* **37,** 1–13 (2009).
55. Huang D. W., Sherman, B. T., Lempicki, R. & A. Systematic and integrative analysis of large gene lists using DAVID bioinformatics resources. *Nature Protocols* **4,** 44–57 (2009).
56. Reverter, A., Hudson, N. J., Nagaraj, S. H., Perez-Enciso, M. & Dalrymple, B. P. Regulatory impact factors: unraveling the transcriptional regulation of complex traits from expression data. *Bioinformatics* **26,** 896–904 (2010).
57. Mailman, M. D. *et al.* The NCBI dbGaP database of genotypes and phenotypes. *Nature Genet.* **39,** 1181–1186 (2007).